From Kondo to local singlet state in graphene nanoribbons with magnetic impurities

G. S. Diniz,[1] G. I. Luiz,[2,3] A. Latgé,[2] and E. Vernek[3]
[1]*Curso de Física, Universidade Federal de Goiás, Jataí, Goiás 75801-615, Brazil*
[2]*Instituto de Física, Universidade Federal Fluminense, Niterói, Rio de Janeiro 24210-340, Brazil*
[3]*Instituto de Física, Universidade Federal de Uberlândia,Uberlândia, Minas Gerais 38400-902, Brazil*

(Received 3 October 2017; revised manuscript received 21 November 2017; published 27 March 2018)

A detailed analysis of the Kondo effect of a magnetic impurity in a zigzag graphene nanoribbon is addressed. An adatom is coupled to the graphene nanoribbon via a hybridization amplitude $\Gamma_{\rm imp}$ in a *hollow*- or *top*-site configuration. In addition, the adatom is also weakly coupled to a metallic scanning tunnel microscope (STM) tip by a hybridization function $\Gamma_{\rm tip}$ that provides a Kondo screening of its magnetic moment. The entire system is described by an Anderson-like Hamiltonian whose low-temperature physics is accessed by employing the numerical renormalization-group approach, which allows us to obtain the thermodynamic properties used to compute the Kondo temperature of the system. We find two screening regimes when the adatom is close to the edge of the zigzag graphene nanoribbon: (1) a weak-coupling regime ($\Gamma_{\rm imp} \ll \Gamma_{\rm tip}$), in which the edge states produce an enhancement of the Kondo temperature T_K, and (2) a strong-coupling regime ($\Gamma_{\rm imp} \gg \Gamma_{\rm tip}$), in which a local singlet is formed, to the detriment of the Kondo screening by the STM tip. These two regimes can be clearly distinguished by the dependence of their characteristic temperature T^* on the coupling between the adatom and the carbon sites of the graphene nanoribbon $V_{\rm imp}$. We observe that in the weak-coupling regime T^* increases exponentially with $V_{\rm imp}^2$. Differently, in the strong-coupling regime, T^* increases linearly with $V_{\rm imp}^2$.

DOI: 10.1103/PhysRevB.97.115444

I. INTRODUCTION

Magnetic impurities embedded in a metallic environment exhibit the paradigmatic many-body phenomenon, the so-called Kondo effect (KE) [1]. Since its explanation in a seminal work by Kondo [2], this effect has been studied in a variety of different physical systems in all dimensionalities (three-, two-, and one-dimensional systems) [3–7]. The capability of manipulating atoms and molecules on metallic surfaces with the aid of a scanning tunnel microscope (STM) tip has renewed the interest in the KE in reduced dimensions, as we have witnessed in the last 20 years [8]. In fact, the advent of the STM has paved the way to a variety of possibilities for investigating the KE in a controllable way in many different systems [9–11]. The great number of theoretical and experimental studies has proved that the observable physical signature of the KE depends drastically on the bare local density of states of the host system.

To understand the dependence of the Kondo physics on the density of states of the free electrons surrounding the magnetic impurities, recall that the physical mechanism underlying the KE is the *dynamical screening* of the localized magnetic moments of the impurities by the conduction electrons of the host material. This screening is led by an effective antiferromagnetic exchange coupling J between the impurity and the surrounding electrons that allows for spin-flip scattering processes involving energies below $k_B T_K$, where k_B is the Boltzmann constant and T_K is the characteristic Kondo temperature. Since these are spin-flip scattering events occurring at low temperatures, they depend strongly on the low-energy density of states (DOS) of the electrons near the localized magnetic moments. This is why metallic systems with a nearly constant density of states around the Fermi level E_F [$\rho(E) = \rho_F$] exhibits a typical Kondo temperature $T_K \propto \exp(-1/\rho_F J)$ but can deviate drastically from this expression if ρ presents important features for E close to E_F. Within the single-impurity Anderson model for spin-1/2 magnetic impurity problems [12], the important quantity entering the expression for T_K is the ratio $U/\Delta(E_F)$, where $\Delta(E) \propto \rho(E)$ is the effective hybridization function and U is the Coulomb repulsion energy at the impurity site. Again, we see that $\rho(E)$ can greatly affect T_K. It is crucially important to explain why T_K is enhanced in peaked effective hybridization functions and vanishing for pseudogapped ones, as discussed for a double-quantum-dot structure [13].

A natural two-dimensional system exhibiting an interesting density of states near the Fermi level is graphene [14–17]. The Dirac cones of the band structure lead to a zero-gap density of states $\rho(E) \propto |E|$, resulting in a rich phase diagram with interesting quantum phase transitions [18,19]. There have been great efforts devoted to the Kondo physics in graphene with an impurity coupled to [18–28] or a vacancy (defect) in the graphene lattice [29–33] in recent years. Surprisingly, much less attention has been paid to the KE on graphene nanoribbons [34]. A graphene nanoribbon (GNR) is formed by breaking the translational symmetry of a graphene sheet in one particular direction. There are two common directions for *cutting* the graphene with well-defined edge shapes: zigzag (ZGNR) and armchair (AGNR). ZGNRs are particularly interesting because around $k = \pi$ they exhibit simultaneously dispersive bulk and bound edge states [35,36]. These bound edge states render a strongly peaked local density of states, as depicted in Fig. 1(c).

Because of the sharp peak in the local density of states, if we place a magnetic impurity near one edge of the ZGNR, we can expect an important modification of the Kondo physics

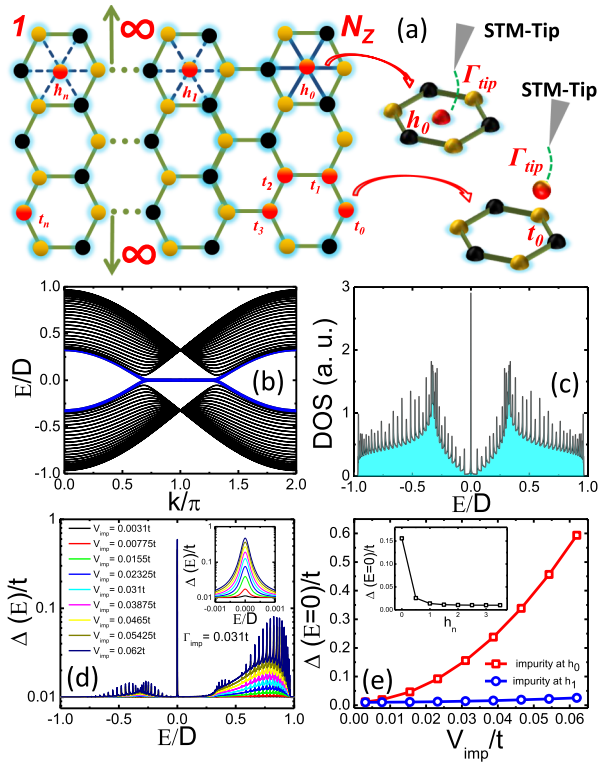

FIG. 1. (a) Schematic representation of N_z-ZGNR with an impurity located at the hollow-site position h_n or at the top-site position t_n. The drawing on the right represents a STM tip on the top of the impurity adatom with a coupling strength $\Gamma_{\rm tip}$. (b) Electronic structure of a pristine 26-ZGNR highlighting the edge states (blue line). (c) DOS as a function of E for pure graphene. (d) Hybridization function $\Delta(E)$ for different values of impurity coupling strength $V_{\rm imp}$ at the h_0 position. Inset: zoom close to $E = 0$ that shows the evolution of the $\Delta(E = 0)$ peak as $V_{\rm imp}$ is enhanced. (e) $\Delta(E = 0)$ for two different impurity locations, h_0 and h_1, as a function of $V_{\rm imp}$. Inset: $\Delta(E = 0)$ vs different adatom positions h_n for $V_{\rm imp} = 0.031t$.

of the system. In particular, in view of the discussion above, we can expect this peak to enhance the Kondo temperature of the system. Recent theoretical density functional theory (DFT) calculations predict that adatoms are possible generators of localized magnetic moments in graphene and GNR at hollow- and top-site positions [34,37–44]. Motivated by these findings, in this work we are interested in investigating the KE of a magnetic impurity placed at two distinct positions in a ZGNR: a hollow site and a top site [45–47]. We employ a numerical renormalization-group (NRG) approach [48,49] to address this problem. More precisely, using the NRG approach we calculate the entropy and magnetic susceptibility (from which we can extract the Kondo temperature with the aid of Wilson's criteria) of the system for an impurity placed at the hollow site for distinct locations along the transversal direction. We find a strong enhancement of T_K when the impurity approaches the edge of the ZGNR. More interestingly, in the strong-coupling regime between the impurity and the nearby carbon atoms, our calculations suggest that the impurity magnetic moment forms a local singlet state with the edge state of the ZGNR.

This paper is structured as follows: in Sec. II we present the theoretical model describing the hybridization function and the numerical renormalization-group approach. In Sec. III the numerical results are discussed. Finally, in Sec. IV we present our conclusions.

II. THEORETICAL MODEL AND METHOD

The system is schematically illustrated in Fig. 1(a) for a N_Z-ZGNR, with the index N_Z standing for the number of zigzag chains in the transversal direction. To model the single magnetic impurity hosted in the GNR (at the hollow site or at the top-site position), we have used the Anderson-like Hamiltonian [12]

$$H = H_{\rm GNR} + H_{\rm imp} + H_{\rm tip} + H_{\rm GNR-imp} + H_{\rm imp-tip}, \qquad (1)$$

where the first term describes the GNR that is modeled by a nearest-neighbor (NN) tight-binding Hamiltonian

$$H_{\rm GNR} = \sum_{i\sigma}(\varepsilon_0 - \mu)c^\dagger_{i\sigma}c_{i\sigma} - t\sum_{\langle i,j\rangle,\sigma} c^\dagger_{i\sigma}c_{j\sigma}, \qquad (2)$$

in which the operator $c^\dagger_{i\sigma}$ ($c_{i\sigma}$) creates (annihilates) an electron with energy ε_0 and spin σ in the ith carbon site of the GNR and μ is the chemical potential that can be externally tuned by a back gate. The matrix element t allows the electron to hop between nearest-neighbor carbon sites [16]. The second term in Eq. (1) describes the single-level Anderson impurity that is modeled by the interacting Hamiltonian $H_{\rm imp} = \varepsilon_d n_{d\sigma} + U n_{d\uparrow} n_{d\downarrow}$, where $d^\dagger_\sigma$ (d_σ) creates (annihilates) an electron with energy ε_d and spin σ at the impurity site, U is the on-site Coulomb interaction, and $n_d = n_{d\uparrow} + n_{d\downarrow}$ (with $n_{d\sigma} \equiv d^\dagger_\sigma d_\sigma$) is the total number operator for the impurity electrons. The third term in Eq. (1) describes the STM tip modeled by the Hamiltonian $H_{\rm tip} = \sum_{\mathbf{k}} \varepsilon_{\mathbf{k}} c^\dagger_{\mathbf{k}\sigma} c_{\mathbf{k}\sigma}$, where $c^\dagger_{\mathbf{k}\sigma}$ ($c_{\mathbf{k}\sigma}$) creates (annihilates) an electron with momentum $\mathbf{k}$ and spin σ in the STM tip. Finally, the last two terms of Eq. (1) couple the impurity to the GNR and to the STM tip, respectively. They are, respectively, given by

$$H_{\rm GNR-imp} = \sum_{j,\sigma} V_j c^\dagger_{j\sigma} d_\sigma \qquad (3)$$

and

$$H_{\rm imp-tip} = \sum_{\mathbf{k}\sigma}(V_{\mathbf{k}} c^\dagger_{\mathbf{k}\sigma} d_\sigma + \text{H.c.}). \qquad (4)$$

In Eq. (3) V_j represents the impurity coupling amplitude of the neighboring carbon atoms (later, we set $V_j \equiv V_{\rm imp}$). For the impurity located at the hollow-site position h_n, the sum in j runs over the six carbon atoms closest to the impurity, while for the top-site position t_n, it corresponds only to the single carbon atom to which the impurity is coupled.

A. Hybridization function

The implementation of the NRG to determine the Kondo temperature of the system requires first the determination of the hybridization function $\Delta(E)$ of the impurity. We do it by using the Green's function method in the noninteracting case ($U = 0$). As the impurity is coupled to both the GNR and the STM tip, we write $\Delta(E) = \Delta_{\rm tip}(E) + \Delta_{\rm GNR}(E)$. To obtain $\Delta_{\rm tip}(E)$ we model the STM tip with a constant density of states ρ_{tip} and assume a coupling, $V_{\mathbf{k}} = V_{\rm tip}$ (independent

of k), so that we can write $\Delta_{\rm tip}(E) = \pi V_{\rm tip}^2 \rho_{\rm tip} \equiv \Gamma_{\rm tip}$. To obtain $\Delta_{\rm GNR}(E)$ we have implemented the standard surface Green's function approach [50,51]. The GNR is then divided into three regions: left lead, central region (where the impurity adatom is located), and right lead. The retarded Green's function matrix of the central region is $G_C(E) = (E + i\eta - H_C - \Sigma_L - \Sigma_R)^{-1}$ (omitting the spin indices), with E being the energy of the injected electron (the Fermi energy at a given doping) and $\eta \to 0$. Here, H_C represents the Hamiltonian describing the central region, and $\Sigma_{L/R}$ are the self-energies that describe the influence of the left/right leads. Explicitly, $\Sigma_l = H_{lC}^\dagger g_l H_{lC}$, where g_l is the Green's function for the $l = L, R$ semi-infinite lead obtained through an iterative procedure of the tight-binding Hamiltonian [50] and H_{lC} couples each lead to the central region. With the Green's function, we can obtain the self-energy of the impurity site $\Delta_{\rm GNR}(E) = {\rm Im}[G_C^{-1}(E)]_{NN}$, where N represents the impurity site inside the central region.

Different from the graphene case, in which for the impurity located at the top site $\Delta(E)$ is a linear function of $|E|$ (or of $|E|^3$ for the hollow site) [19,52], in the ZGNR $\Delta(E)$ displays a much more complex dependence on E. In the ZGNR, for instance, the presence of the edge state dramatically alters the hybridization function $\Delta(E)$. To illustrate this, in Fig. 1(b) we show the electronic structure of a 26-ZGNR (where 26 indicates the number of zigzag chains along the transverse direction). The blue curve corresponds to the edge states. Note that it exhibits a flat zero-energy plateau around $k = \pi$. This plateau gives rise to a sharp zero-energy peak in the DOS of the pristine 26-ZGNR (in the absence of the impurity), $\rho_{\rm GNR}^{(0)}(E) = {\rm Im\,Tr}[G_c^{(0)}(E)]$, as shown in Fig. 1(c).

Since the sharp contribution to $\rho_{\rm GNR}^{(0)}(E)$ is located at the edges of the ZGNR, for the impurity coupled to the carbon atoms close to the edges a strong enhanced hybridization is observed at $E = 0$, as shown in Fig. 1(d). Also, we can notice that several satellite peaks appear as a consequence of the Van Hove singularities in the DOS of the ZGNR [35,36]. Interestingly, note that while $\rho_{\rm GNR}^{(0)}(E)$ [Fig. 1(c)] is particle-hole symmetric, $\Delta(E)$ [Fig. 1(d)] is not. This is because while the former is calculated in the absence of the impurity, the latter is defined with the impurity coupled to the GNR, which for the hollow site breaks the particle-hole symmetry of the system, a known behavior of nonbipartite lattices [53,54]. By increasing the impurity coupling $V_{\rm imp}$, the zero-energy peak of $\Delta(E = 0)$ also increases. This is better appreciated in the inset of Fig. 1(d). In Fig. 1(e) we show $\Delta(E)$ vs $V_{\rm imp}$ for the impurity placed at h_0 (red squares) and h_1 (blue circles). We first note that $\Delta(E = 0)$ is much larger for the impurity at position h_0 than in position h_1 [see the inset of Fig. 1(e)] for $V_{\rm imp} = 0.031t$, which is consistent with the expected decay of the edge-state wave function across the ribbon width [55]. Moreover, we can observe that $\Delta(0) \propto V_{\rm imp}^2$, similar to the case of an impurity coupled to a metallic surface [12].

For the sake of completeness, we have also analyzed a metallic AGNR with an adatom at the hollow site, with a width similar to that of the 26-ZGNR. For this purpose, we choose the 47-AGNR, which means 47 N_A (dimers line) along the transversal direction [35]. However, we find no significant change in the local DOS close to the Fermi level or, consequently, for the hybridization function around $E = 0$ for different adatom impurity positions along the transversal direction. This is a consequence of the almost flat density of states around $E = 0$ and the absence of edge states in the AGNR [35]. For metallic AGNR close to the Fermi level, we expect the Kondo physics to mimic the case of a magnetic impurity hosted in a normal metal, where a nearly constant density of states is expected.

B. Numerical renormalization-group approach

To provide the Kondo physics description of the GNR with an impurity adatom, we use Wilson's NRG approach [48,49]. For this purpose, we set Wilson's discretization parameter as $\Lambda = 2.0$, retaining 2000 many-body states after each iteration and using the z averaging in the interval $0.2 \leqslant z \leqslant 1.0$ in steps of 0.2 [56]. The entropy is obtained within the canonical ensemble as $S(T) = \beta\langle H\rangle + \ln Z$, where Z corresponds to the number of occupied states and $\beta = 1/k_B T$. Similarly, the magnetic moment is given by $Z^{-1}\Sigma_n[\langle\Psi_n|S_z^2|\Psi_n\rangle - \langle\Psi_n|S_z|\Psi_n\rangle]e^{-\beta E_n}$. It is important to mention that we seek the entropy $S_{\rm imp}$ and magnetic moment $\chi_{\rm imp}$ which correspond (approximately) to the contribution of impurity to the entropy and to the magnetic moment and are defined as the difference of the thermodynamical quantities computed for the total Hamiltonian H (with the impurity) and with H_0 (without the impurity). Further technical details can be found, for instance, in Ref. [49] and references therein.

III. NUMERICAL RESULTS

The following results are for the N_Z-ZGNR. To obtain our numerical results, we choose the hopping t such that the half bandwidth is unity, i.e., $D = 1$, and can be used as our energy unity. With this in mind, we use $U/t = 1$ and $\Gamma_{\rm tip} = 0.031t$ for all calculations. With this choice, for $V_{\rm imp} = 0$, the hybridization of the impurity with the STM tip will render a very small Kondo temperature (which depends essentially on the ratio $U/\Gamma_{\rm tip} \approx 32.3$) that can be estimated by [57] $k_B T_K \approx \sqrt{\Gamma_{\rm tip} U}\, e^{-\pi U/8\Gamma_{\rm tip}} \approx 5.5 \times 10^{-7} t$ for $\delta = 0$, where $\delta = \varepsilon_d + U/2$. Numerically, T_K is obtained from the magnetic moment, following Wilson's criteria [48], $k_B T_K \chi(T_K)/(g\mu_B^2) = 0.0707$, where g is the Landé g factor and μ_B is the Bohr magneton. With this prescription we find (for $V_{\rm imp} = 0$) $k_B T_K \approx 9.6 \times 10^{-8} t \equiv k_B T_K^{(0)}$ (this will be used later to rescale our characteristic temperatures).

A. Hollow-site adatom

To study the effect of the edge state on the Kondo physics screening of the system we first focus on the hollow-site position. In Fig. 2 we show the entropy (top) and the magnetic moment (bottom) as a function of temperature for different N_Z-ZGNR for $V_{\rm imp} = 0.0155t$, $\delta/U = 0$, and the impurity located at h_0 (left) and h_1 (right). Overall, the features observed for $S_{\rm imp}(T)$ and $k_B T\,\chi_{\rm imp}(T)$ are similar to those known for the traditional single Anderson impurity problem. As shown in Fig. 2(a), we see two drops in $S_{\rm imp}(T)$ as T decreases. The first corresponds to the crossover from the free orbital to the local-moment regime, while the second one corresponds to

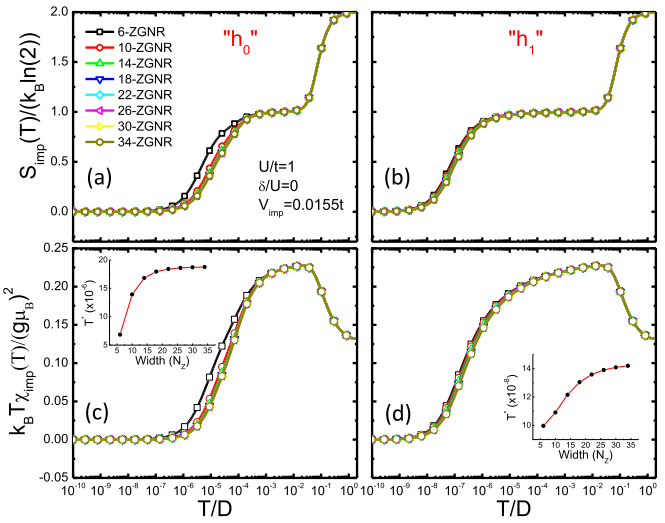

FIG. 2. (a) and (b) Entropy and (c) and (d) magnetic moment vs T for the impurity located at h_0 (left) and h_1 (right) for different widths of the ZGNR. For all panels, $\delta/U = 0, U/t = 1$, and $V_{\rm imp} = 0.0155t$. The insets of (c) and (d) show the characteristic Kondo temperature T^* vs N_Z for the corresponding adatom position.

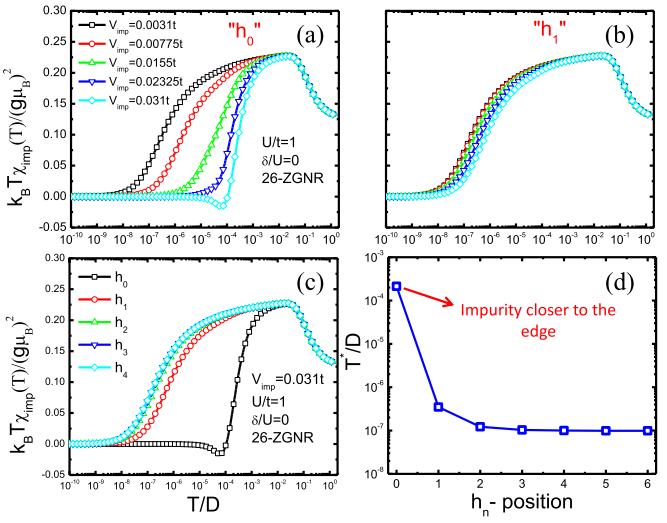

FIG. 3. Magnetic moment vs temperature for the impurity located at (a) h_0 and (b) h_1 and for various values of $V_{\rm imp}$. (c) Magnetic moment vs temperature for different positions of the adatom h_n with a fixed value of $V_{\rm imp} = 0.031t$. (d) Kondo temperature T^* vs position h_n ($n = 0,1,\ldots,6$), with $V_{\rm imp} = 0.031t$. Notice that in this panel we have set the vertical axis on a log scale.

the quench of the local magnetic moment by the conduction electrons, which characterizes the onset of the KE. Similarly, the magnetic moment follows the same feature observed in the single Anderson impurity embedded in a metal. What is interesting here is that, for a given position of the impurity h_0 (left) or h_1 (right), as N_Z increases, $S_{\rm imp}$ and $k_BT\chi_{\rm imp}$ drop to zero at higher temperatures. This suggests that the *sharpening* of the edge state for increasing N_Z enhances the Kondo temperature of the system. The insets of Figs. 2(c) and 2(d) show the characteristic temperature T^* vs N_Z for positions h_0 and h_1, respectively. According to our previous discussion, note that for a given position of the impurity, h_0 or h_1, T^* with N_Z increases and saturates to a given value. Observe also that consistent with the exponential decay of the wave function as it penetrates across the ZGNR width [35], T^* is much larger for the impurity placed at h_0 [Fig. 2(c)] than for the situation in which it is placed at h_1 [Fig. 2(d)]. For the results shown so far we fixed $V_{\rm imp}$ at a small value ($0.0155t$). This ensures that even the strongest influence of the edge state of the ZGNR occurring for the position h_0 does not change the picture of the Kondo screening.

We address the question of whether this picture remains valid for a magnetic impurity in a tighter connection to the ZGNR. To do so, let us turn our attention to the dependence of the magnetic moment suppression as we increase $V_{\rm imp}$ for a given impurity position. Here, we focus on the 26-ZGNR with the adatom at the hollow-site position, for which T^* is almost converged [especially for an impurity adatom located at the edge; see the insets of Figs. 2(c) and 2(d)]. Since the drop in $k_BT\chi_{\rm imp}$ corresponds to a drop in $S_{\rm imp}$, it suffices to discuss only one of them. Therefore, from now on we will discuss only $k_BT\chi_{\rm imp}$. In Figs. 3(a) and 3(b) we show the impurity magnetic susceptibility $k_BT\chi_{\rm imp}$ vs T for different values of $V_{\rm imp}$ for an impurity placed at h_0 and h_1, respectively. First, by comparing the curves of Fig. 3(a) with those of Fig. 3(b) we observe that the quenching of the magnetic moments is much more strongly dependent on $V_{\rm imp}$ for h_0 than for the h_1 position. Again, this is because the closer the impurity is to the ZGNR edge, the stronger the hybridization of the impurity orbital with the edge state is. This also can be seen in Fig. 3(c), which shows $k_B\chi_{\rm imp}$ vs T for different positions of the impurity on the 26-GNR. Note that the quench of the magnetic moment occurs at a much higher temperature for position h_0 than for the other positions. As the impurity is moved far away from the edge, the curves of $k_BT\chi_{\rm imp}$ rapidly collapse onto each other, approaching the one for $V_{\rm imp} = 0$. This is because far away from the edge the KE is essentially due to the STM tip. Using the same Wilson's criteria, from the results of Fig. 3(c) we extract the characteristic temperature T^* below which the magnetic moment is quenched. The results are shown in Fig. 3(d) as T^* vs h_n for fixed $V_{\rm imp} = 0.031t$. We can observe that T^* drops about three orders of magnitude as the impurity moves from h_0 to h_3. Remarkably, the results for the impurity position h_0 [black curve in Fig. 3(c)] differ significantly from the others, exhibiting a dramatic magnetic moment suppression. The natural question to raise is whether this suppression happening for h_0 and large $V_{\rm imp}$ is of the Kondo type. To answer this question, we show in Fig. 4 $T^*/T_K^{(0)}$ vs $V_{\rm imp}^2$ for two different adatom locations, at the hollow-site position h_0 in Fig. 4(a) and at h_1 in Fig. 4(b), for different values of δ/U. From Fig. 4(a) we can clearly distinguish two different regimes: for large $V_{\rm imp}$ we note a linear behavior of T^* with $V_{\rm imp}^2$, but for small $V_{\rm imp}$ the dependence seems to be exponential. This is better seen in the inset of Fig. 4(a). To understand this, let us remember that when the impurity is coupled to both the tip and the ZGNR, the effective hybridization is given by $\Gamma = \Gamma_{\rm tip} + \Gamma_{\rm imp}$. Here, $\Gamma_{\rm imp} = aV_{\rm imp}^2$, where a is a constant that depends on the position of the impurity and the local density of states of the ZGNR. In the small-$V_{\rm imp}$ regime we can use the expression for

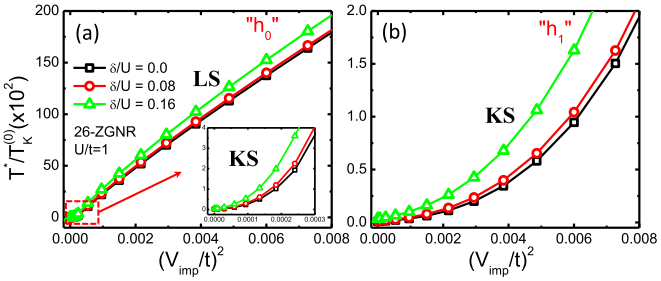

FIG. 4. $T^*/T_K^{(0)}$ as a function of $(V_{\rm imp}/t)^2$ for (a) h_0 and (b) h_1 for different δ/U ratios. The inset of (a) shows a zoom of the region of small values of $(V_{\rm imp}/t)^2$. The parameters used are in the legend of (a) and $T_K^{(0)} = 9.6 \times 10^{-8} t$.

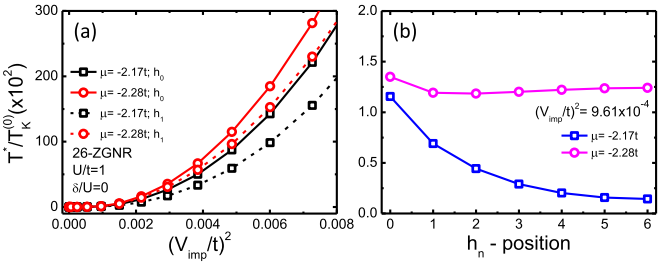

FIG. 5. (a) $T^*/T_K^{(0)}$ vs $(V_{\rm imp}/t)^2$ for $\mu = -2.17t$ (black) and $-2.28t$ (red) and h_0 (solid lines) and h_1 (dashed lines) and (b) T^* vs adatom position h_n ($n = 0, \ldots, 6$), with $(V_{\rm imp}/t)^2 = 9.61 \times 10^{-4}$. The other parameters are $\delta = 0$ and $U = t$. Here, $T_K^{(0)} = 9.6 \times 10^{-8} t$.

T_K for T^*. Therefore,

$$T^* \sim e^{-\pi U/8\Gamma}. \tag{5}$$

For $\Gamma_{\rm imp} \ll \Gamma_{\rm tip}$ we can write

$$\frac{1}{\Gamma} \approx \frac{1}{\Gamma_{\rm tip}}\left(1 - \frac{\Gamma_{\rm imp}}{\Gamma_{\rm tip}}\right). \tag{6}$$

Thus, we obtain

$$T^* \sim e^{-\pi U/8\Gamma_{\rm tip}} e^{(\pi U/8\Gamma_{\rm tip}^2)\Gamma_{\rm imp}} \sim T_K^{(0)} e^{bV_{\rm imp}^2}, \tag{7}$$

where $T_K^{(0)}$ is the Kondo temperature for $V_{\rm imp} = 0$ and $b = \pi U a/8\Gamma_{\rm tip}^2$. Note that expression (7) is consistent with the exponential behavior of T^* shown in the inset of Fig. 4(a). This shows indeed that in the regime of small $V_{\rm imp}$ the quenching of the magnetic moment is actually of the Kondo type; therefore, we call it the Kondo singlet (KS) regime, so T^* can be identified as T_K.

In contrast, in the opposite regime the behavior of T^* can no longer be understood within the picture described above. In this case, the strong coupling between the impurity and the bound edge state (for position h_0) induces the formation of a local singlet (LS). Within this picture, the impurity and the edge state can now be thought of as two hybridized electronic levels with Coulomb repulsion U in one of them. The energy gain to form a LS state in this simple system is known to be $E_S = -4V_{\rm imp}^2/U$. This explain why in the strong impurity-ZGNR coupling regime $T^* \propto V_{\rm imp}^2$. In this case, we prefer not to identify T^* as T_K since here the singlet does not involve the Fermi sea as in the traditional KE. This is actually akin to what was discussed by one of us in Ref. [58]. If we now look at Fig. 4(b), this linear behavior of T^* with $V_{\rm imp}^2$ is not observed (at least for the range of $V_{\rm imp}$ shown). This is because at position h_1 the influence of the edge state on the impurity remains a small perturbation. Interestingly, as we observe similar behavior of the different curves in Fig. 5, the two regimes discussed above remain clearly distinguishable for $\delta \neq 0$.

As we have seen above, the behavior of $T^* \sim V_{\rm imp}^2$ can be nicely understood in terms of the local singlet formed by the impurity and the states bound to the edge of the ZGNR. We can argue that if we tune the chemical potential close to a Van Hove singularity, this behavior would no longer be seen. This is because the Van Hove singularities are not directly associated with states bound to the edges. To confirm this, we now consider the chemical potential μ at two different Van Hove singularities with a relative peak similar to the edge state and calculate T^*. In Fig. 5(a) we show T^* vs $V_{\rm imp}^2$ for $\mu = -2.17t$ (black) and $\mu = -2.28t$ (red) for the two impurity positions, h_0 (solid lines) and h_1 (dashed lines). Notice that for all cases T^* increases exponentially with $V_{\rm imp}^2$, very similar to the results shown in Fig. 4(b) and in the inset of Fig. 4(a). Confirming our prediction, this shows that in this case, the coupling to the ZGNR no longer favors a LS but leads to a KS state with an enhanced T_K. In Fig. 5(b) we show T^* as a function of the impurity position h_n for the two different chemical potentials used in Fig. 5(a). As we see, T^* still decreases quite substantially for $\mu = -2.17t$ (blue squares), but for $\mu = -2.28t$ (magenta circles) it is almost as if the impurity moves far away from the edge. This can be understood based on the fact the electronic states that contribute more to the higher-energy Van Hove singularities are more extended across the ZGNR.

B. Top-site adatom

We now investigate whether the two screening regimes discussed above also occur for the adatom placed in a top-site position. The results obtained in this case are shown in Fig. 6. Figure 6(a) shows $k_B T \chi_{\rm imp}$ vs temperature for different positions t_n and for a fixed value of $V_{\rm imp} = 0.031t$ [as in Fig. 3(c)]. Like for the hollow-site positions, we note that the characteristic temperature T^* (where $k_B T \chi_{\rm imp}$ drops to zero) increases as the impurity adatom approaches the edge of the ZGNR. Also, like in the hollow-site case, a dramatic change in the shape of the $k_B T \chi_{\rm imp}$ curve occurs for t_0 compared to the others. This change in regime is accompanied by a dramatic drop in T^*, as shown in Fig. 6(b), which shows T^* vs t_n. Interestingly, we note that T^* exhibits a damping oscillation as the adatom moves away from the ZGNR edge. This behavior was not observed for the hollow-site positions. This difference can be understood as follows: in the hollow-site case, the adatom couples equally to all six carbon atoms of the hexagon. Hence, the contribution from these neighboring atoms to the corresponding hybridization function is somehow *averaged* over the different connected carbon atoms (of the A and B sublattices). On the other hand, in top-site positions, the total contribution to the hybridization function comes solely from a single carbon atom (of the A or B sublattice). Therefore, the systematic oscillation with an exponential decay in the local DOS as observed across the ZGNR [35,36] directly influences

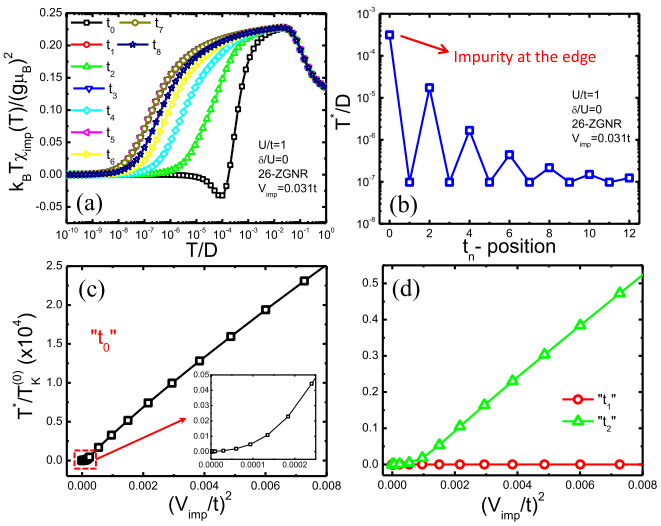

FIG. 6. (a) Magnetic moment vs T for the impurity located at different top-site positions t_n. (b) Characteristic temperature T^* vs t_n for $V_{\rm imp} = 0.031t$ [the same as in Fig. 3(d)]. T^* vs $(V_{\rm imp}/t)^2$ for the impurity at (a) position t_0 and (b) positions t_1 and t_2.

the hybridization function $\Delta(E)$. In Fig. 6(c) we show T^* vs $V_{\rm imp}^2$ for position t_0, and in Fig. 6(d) we show the same for positions t_1 and t_2. We clearly note a linear behavior of T^* for large $V_{\rm imp}$ for both t_0 and t_2. Also, for the t_0 adatom position (and the subsequent t_{2*n}) we see an exponential behavior of T^* for small $V_{\rm imp}$. This is better appreciated in the inset of Fig. 6(c), which shows a zoom of the region of small $V_{\rm imp}$ for t_0. For the t_1 position T^* is practically insensitive to changes in $V_{\rm imp}^2$. These results show that the two LS and KS screening regimes indeed occur for both hollow- and top-site positions whenever the adatom is placed close to the edge of the ZGNR.

C. Effect of the next-nearest-neighbor coupling

In this section we show that our results remain robust when we include next-nearest-neighbor (NNN) hopping in our tight-binding model [16,59]. To this end, following Refs. [60,61], we include the NNN in the model [62]. This coupling can be quite important for the armchair GNRs, where a drastic change is expected for the electronic structure close to the Fermi level with the development of a band gap with the appearance of a metallic-insulator transition, as observed in DFT calculations [63]. For the case of ZGNR, small corrections are predicted, but the characteristic edge states are preserved in the NNN approach [64,65]. Therefore, the simplest NN approximation in the previous sections can safely be used [66,67], predicting qualitatively valid results. For completeness, in Fig. 7 we compare the two cases by calculating the hybridization function $\Delta(E)$ and the characteristic temperature T^* for the hollow site configuration. Figure 7(a) shows the hybridization function $\Delta(E)/t$ for the NN (black line) and NNN (red line) approximations. Because of the presence of the impurity in the hollow-site configuration, even for the NN approximation the system is particle-hole asymmetric. However, the central peak remains at $E = 0$ (and approximately symmetric). On the other hand, for the NNN approximation not only is $\Delta(E)$ asymmetric, but also the zero-energy edge state shifts towards

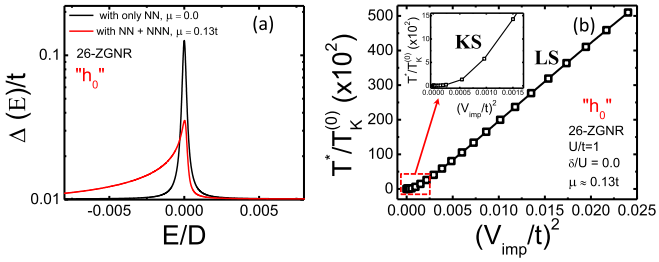

FIG. 7. (a) Hybridization function $\Delta(E)/t$ for different tight-binding approximations with $V_{\rm imp}/t = 0.031$. (b) Characteristic temperature T^* vs $(V_{\rm imp}/t)^2$ for the impurity at position h_0. The inset shows a zoom of the region of low $V_{\rm imp}$. In (a) and (b) we have set a chemical potential of $\mu = 0.13t$ for the NNN.

the valence band [64,68]. Notice that for the NNN we have set $\mu = 0.13t$, so the peak appears at $E = 0$. The particular value of μ depends on the model parameters, with an approximate value of 0.4 eV [16,59,64,69]. The stronger particle-hole asymmetry of the NNN compared to the NN case is because in the NNN approximation the ZGNR bands are themselves particle-hole asymmetric, regardless of the presence of the impurity. Figure 7(b) shows T^* vs $(V_{\rm imp}/t)^2$ for the NNN case. We see that the results are qualitatively equivalent to the NN approximation shown in Fig. 4(a). As expected, only quantitative changes are noted. For the NNN case, the transition from KS to LS occurs at a larger $V_{\rm imp}$, a direct consequence of the height reduction of the central peak in the $\Delta(E)$ function.

IV. CONCLUSION

We have studied the screening effect of a magnetic impurity (adatom) on a ZGNR. The system was described by an Anderson-like Hamiltonian in which the adatom is coupled to the ZGNR as well as to a metallic STM tip. To access the low-temperature physics of the system we have employed a numerical renormalization-group approach that allows us to calculate the relevant physical quantities. In particular, we have calculated the magnetic susceptibility of the system and extracted the characteristic temperature T^*, below which the adatom magnetic moment is screened. We have analyzed both the *hollow*- and *top-site* adatom configurations. We have found two screening regimes of the adatom magnetic moment: (1) a local singlet (LS) when the adatom is *strongly* coupled to the bound edge state of the ZGNR and (2) a Kondo singlet (KS) in the *weak*-coupling case. The system crosses over the LS to the usual KS either as the impurity is moved away from the edge of the ZGNR or when its coupling $V_{\rm imp}$ to the ZGNR is small. These two screening regimes are well defined by the behavior of the characteristic temperature T^* with $V_{\rm imp}$. In the LS regime, T^* increases linearly with $V_{\rm imp}^2$, whereas in the KS it increases exponentially with $V_{\rm imp}^2$. We have shown that in the LS regime, the linear dependence of T^* on $V_{\rm imp}^2$ is consistent with a singlet state formed between the magnetic moment of the impurity and that of an electron in the bound edge state. Interestingly, the KS can be understood in terms of an enhancement of the Kondo temperature as $V_{\rm imp}$ increases. In this sense, in the LS regime the ZGNR state that is bound to the edge competes with the Kondo screening of

the adatom magnetic moment by the conduction electrons of the STM tip, whereas in the KS case, the ribbon extended state cooperates with the Kondo screening by the STM tip. Finally, we have shown that these conclusions remain valid when we considered a more realistic model by adding second-nearest-neighbor hopping in our tight-binding Hamiltonian. Our results are important to the comprehension of the Kondo physics in graphene nanoribbons, and given the relative simplicity of the physical system studied here, we believe that our results can be experimentally accessed via transport properties in STM measurements [70,71].

ACKNOWLEDGMENTS

We thank R. Žitko for his assistance with the NRG LJUBLJANA code [72]. We acknowledge financial support received from CAPES, FAPEMIG, FAPERJ, and CNPq.

[1] A. C. Hewson, *The Kondo Problem to Heavy Fermions* (Cambridge University Press, Cambridge, 1993).
[2] J. Kondo, Prog. Theor. Phys. **32**, 37 (1964).
[3] S. Ernst, S. Kirchner, C. Krellner, C. Geibel, G. Zwicknagl, F. Steglich, and S. Wirth, Nature (London) **474**, 362 (2011).
[4] P. Jarillo-Herrero, J. Kong, H. S. van der Zant, C. Dekker, L. P. Kouwenhoven, and S. De Franceschi, Nature (London) **434**, 484 (2005).
[5] J. Nygard, D. H. Cobden, and P. E. Lindelof, Nature (London) **408**, 342 (2000).
[6] S. Sasaki, S. De Franceschi, J. M. Elzerman, W. G. van der Wiel, M. Eto, S. Tarucha, and L. P. Kouwenhoven, Nature (London) **405**, 764 (2000).
[7] D. Goldhaber-Gordon, H. Shtrikman, D. Mahalu, D. Abusch-Magder, U. Meirav, and M. A. Kastner, Nature (London) **391**, 156 (1998).
[8] L. Kouwenhoven and L. Glazman, Phys. World **14**, 33 (2001).
[9] H. C. Manoharan, C. P. Lutz, and D. M. Eigler, Nature (London) **403**, 512 (2000).
[10] G. A. Fiete, G. Zarand, B. I. Halperin, and Y. Oreg, Phys. Rev. B **66**, 024431 (2002).
[11] V. Iancu, A. Deshpande, and S.-W. Hla, Phys. Rev. Lett. **97**, 266603 (2006).
[12] P. W. Anderson, Phys. Rev. **124**, 41 (1961).
[13] L. G. G. V. Dias da Silva, N. P. Sandler, K. Ingersent, and S. E. Ulloa, Phys. Rev. Lett. **97**, 096603 (2006).
[14] K. S. Novoselov, A. K. Geim, S. V. Morozov, D. Jiang, Y. Zhang, S. V. Dubonos, I. V. Grigorieva, and A. A. Firsov, Science **306**, 666 (2004).
[15] K. S. Novoselov, V. I. Fal'ko, L. Colombo, P. R. Gellert, M. G. Schwab, and K. Kim, Nature (London) **490**, 192 (2012).
[16] A. H. Castro Neto, F. Guinea, N. M. R. Peres, K. S. Novoselov, and A. K. Geim, Rev. Mod. Phys. **81**, 109 (2009).
[17] A. K. Geim and K. S. Novoselov, Nat. Mater. **6**, 183 (2007).
[18] L. Fritz and M. Vojta, Rep. Prog. Phys. **76**, 032501 (2013).
[19] D. A. Ruiz-Tijerina and L. G. G. V. Dias da Silva, Phys. Rev. B **95**, 115408 (2017).
[20] L. Li, Y.-Y. Ni, Y. Zhong, T.-F. Fang, and H.-G. Luo, New J. Phys. **15**, 053018 (2013).
[21] K. Sengupta and G. Baskaran, Phys. Rev. B **77**, 045417 (2008).
[22] T. O. Wehling, A. V. Balatsky, M. I. Katsnelson, A. I. Lichtenstein, and A. Rosch, Phys. Rev. B **81**, 115427 (2010).
[23] S.-P. Chao and V. Aji, Phys. Rev. B **83**, 165449 (2011).
[24] Z.-G. Zhu and J. Berakdar, Phys. Rev. B **84**, 165105 (2011).
[25] J. Jobst, F. Kisslinger, and H. B. Weber, Phys. Rev. B **88**, 155412 (2013).
[26] M. Kharitonov and G. Kotliar, Phys. Rev. B **88**, 201103 (2013).
[27] D. Mastrogiuseppe, A. Wong, K. Ingersent, S. E. Ulloa, and N. Sandler, Phys. Rev. B **90**, 035426 (2014).
[28] E. Kogan, K. Noda, and S. Yunoki, Phys. Rev. B **95**, 165412 (2017).
[29] J.-H. Chen, L. Li, W. G. Cullen, E. D. Williams, and M. S. Fuhrer, Nat. Phys. **7**, 535 (2011).
[30] P. Haase, S. Fuchs, T. Pruschke, H. Ochoa, and F. Guinea, Phys. Rev. B **83**, 241408 (2011).
[31] T. Kanao, H. Matsuura, and M. Ogata, J. Phys. Soc. Jpn. **81**, 063709 (2012).
[32] A. K. Mitchell and L. Fritz, Phys. Rev. B **88**, 075104 (2013).
[33] V. G. Miranda, L. G. G. V. Dias da Silva, and C. H. Lewenkopf, Phys. Rev. B **90**, 201101(R) (2014).
[34] D. Krychowski, J. Kaczkowski, and S. Lipinski, Phys. Rev. B **89**, 035424 (2014).
[35] K. Nakada, M. Fujita, G. Dresselhaus, and M. S. Dresselhaus, Phys. Rev. B **54**, 17954 (1996).
[36] K. Wakabayashi, Y. Takane, M. Yamamoto, and M. Sigrist, New J. Phys. **11**, 095016 (2009).
[37] H. Sevinçli, M. Topsakal, E. Durgun, and S. Ciraci, Phys. Rev. B **77**, 195434 (2008).
[38] H. Johll, H. C. Kang, and E. S. Tok, Phys. Rev. B **79**, 245416 (2009).
[39] E. J. G. Santos, A. Ayuela, and D. Sánchez-Portal, New J. Phys. **12**, 053012 (2010).
[40] M. P. Lima, A. J. R. da Silva, and A. Fazzio, Phys. Rev. B **84**, 245411 (2011).
[41] A. V. Krasheninnikov, P. O. Lehtinen, A. S. Foster, P. Pyykkö, and R. M. Nieminen, Phys. Rev. Lett. **102**, 126807 (2009).
[42] J. Ding, Z. Qiao, W. Feng, Y. Yao, and Q. Niu, Phys. Rev. B **84**, 195444 (2011).
[43] Y. Mao, J. Yuan, and J. Zhong, J. Phys. Condens. Matter **20**, 115209 (2008).
[44] M. Mashkoori and S. A. Jafari, J. Phys. Condens. Matter **27**, 156001 (2015).
[45] T. Eelbo, M. Waśniowska, P. Thakur, M. Gyamfi, B. Sachs, T. O. Wehling, S. Forti, U. Starke, C. Tieg, A. I. Lichtenstein, and R. Wiesendanger, Phys. Rev. Lett. **110**, 136804 (2013).
[46] F. Donati, Q. Dubout, G. Autès, F. Patthey, F. Calleja, P. Gambardella, O. V. Yazyev, and H. Brune, Phys. Rev. Lett. **111**, 236801 (2013).
[47] H. González-Herrero, J. M. Gómez-Rodríguez, P. Mallet, M. Moaied, J. J. Palacios, C. Salgado, M. M. Ugeda, J.-Y. Veuillen, F. Yndurain, and I. Brihuega, Science **352**, 437 (2016).
[48] K. G. Wilson, Rev. Mod. Phys. **47**, 773 (1975).
[49] R. Bulla, T. A. Costi, and T. Pruschke, Rev. Mod. Phys. **80**, 395 (2008).

[50] M. Buongiorno Nardelli, Phys. Rev. B **60**, 7828 (1999).
[51] M. P. L. Sancho, J. M. L. Sancho, and J. Rubio, J. Phys. F **14**, 1205 (1984).
[52] B. Uchoa, T. G. Rappoport, and A. H. Castro Neto, Phys. Rev. Lett. **106**, 016801 (2011).
[53] E. Müller-Hartmann, J. Low Temp. Phys. **99**, 349 (1995).
[54] D. O. Demchenko, A. V. Joura, and J. K. Freericks, Phys. Rev. Lett. **92**, 216401 (2004).
[55] We have also calculated $\Delta(E=0)$ for the adatom located at the nearest neighboring hexagon, i.e., an adatom at the hollow-site position between h_n and h_{n+1}. As expected, the result for $\Delta(E=0)$ is an intermediate value. Therefore, in the NRG calculations we have considered only h_n positions, as shown in Fig. 1(a), without loss of generality for the thermodynamical results.
[56] R. Žitko and T. Pruschke, Phys. Rev. B **79**, 085106 (2009).
[57] F. D. M. Haldane, Phys. Rev. Lett. **40**, 416 (1978).
[58] E. Vernek, P. A. Orellana, and S. E. Ulloa, Phys. Rev. B **82**, 165304 (2010).
[59] S. Reich, J. Maultzsch, C. Thomsen, and P. Ordejón, Phys. Rev. B **66**, 035412 (2002).
[60] A. Lherbier, A. R. Botello-Méndez, and J.-C. Charlier, Nano Lett. **13**, 1446 (2013).
[61] A. Lherbier, S. M.-M. Dubois, X. Declerck, Y.-M. Niquet, S. Roche, and J.-C. Charlier, Phys. Rev. B **86**, 075402 (2012).
[62] The NNN interaction was considered by adding the term $H_{\mathrm{NNN}} = t' \sum_{\langle\langle i,j\rangle\rangle,\sigma} c^{\dagger}_{i\sigma} c_{j\sigma}$ to the Hamiltonian of Eq. (2), where t' is the hopping amplitude for the second-nearest neighbors.
[63] Y.-W. Son, M. L. Cohen, and S. G. Louie, Phys. Rev. Lett. **97**, 216803 (2006).
[64] Y. Hancock, A. Uppstu, K. Saloriutta, A. Harju, and M. J. Puska, Phys. Rev. B **81**, 245402 (2010).
[65] T. G. Pedersen, Phys. Rev. B **91**, 085428 (2015).
[66] T. Aktor, A.-P. Jauho, and S. R. Power, Phys. Rev. B **93**, 035446 (2016).
[67] I. Martin and Y. M. Blanter, Phys. Rev. B **79**, 235132 (2009).
[68] V.-T. Tran, J. Saint-Martin, P. Dollfus, and S. Volz, AIP Adv. **7**, 075212 (2017).
[69] R. S. Deacon, K.-C. Chuang, R. J. Nicholas, K. S. Novoselov, and A. K. Geim, Phys. Rev. B **76**, 081406 (2007).
[70] D. Goldhaber-Gordon, J. Göres, M. A. Kastner, H. Shtrikman, D. Mahalu, and U. Meirav, Phys. Rev. Lett. **81**, 5225 (1998).
[71] P. Wahl, L. Diekhöner, M. A. Schneider, L. Vitali, G. Wittich, and K. Kern, Phys. Rev. Lett. **93**, 176603 (2004).
[72] R. Žitko, NRG LJUBLJANA, open source NRG code, http://nrgljubljana.ijs.si.